59th ILMENAU SCIENTIFIC COLLOQUIUM
Technische Universität Ilmenau, 11 – 15 September 2017
URN: urn:nbn:de:gbv:ilm1-2017iwk-021:0

Nano-optical quarter-wave plates for applications in the visible wavelength regime: fabrication, tolerances and in-situ process control

Carsten Stock[a,c], Thomas Siefke[a,b], Uwe Zeitner[a,c], Ernst-Bernhard Kley[a]

[a] Friedrich-Schiller-University Jena, Institute of Applied Physics, Albert-Einstein-Str. 15, Jena, 07745, Germany; [b] Physikalisch-Teschnische Bundesanstalt Braunschweig, Bundesallee 100, Braunschweig, 38116, Germany; [c] Fraunhofer Institute of Applied Optics and Precision Engineering, Albert-Einstein-Str. 7, Jena, 07745, Germany

ABSTRACT

The controlling of the polarization state of light is required for various photonic applications, e.g. for biomedical imaging, lithography, microscopy or ellipsometry. Major advantages of micro- and nanostructures for polarization control are realization of elements for spectral bands, where no alternatives exist (e.g. polarizers in the UV wavelength range) and better integration with optical elements or sensors. Nano-optical polarizers and wave plates can be used to fully manipulate and convert the state of polarization. The fabrication of sub-wavelength grating quarter-wave plates for applications in the visible and near infrared wavelength regime is challenging. In this work major grating structure deviations, namely grating ridge tilt, chamfers on top of the ridges, grating displacement and their influence on phase retardation are investigated. Basing on this we present theoretical investigations and experimental results for an in-situ process control. Thereby, the impact of structure deviations can be compensated and a fine tuning of the phase retardation becomes feasible. We demonstrate this approach by fabrication of a wave plate for 532nm wavelength. This work is the foundation for future development of such an in-situ process control.

INTRODUCTION

Optical devices are continuously decreasing in size requiring even smaller optical elements. Classical bulk-optic-based elements are limited in their dimensions, overall shape and integration with other optical components. Micro- and nano-optical elements can surpass these limitations and facilitate multi-functional applications by combination of multiple elements [1, 2]. Due to well-established mass production processes the fabrication costs of micro- and nano-optical elements can be reduced. By nano-optical wire grid polarizers and wave plates, which are here realized as sub-wavelength gratings, the polarization properties of light can be fully controlled. These elements can be understood as effective dichroic or birefringent layers. Typically wire grid polarizers transmit TM polarized light (transversal magnetic-electrical field oscillating orthogonal to the grating ridges) and block the transmission of TE polarized light (transversal electric-electrical field oscillating parallel to the grating ridges). Many experiences are available for the design and fabrication of such elements [3]–[5]. Wave plates retard the orthogonal polarization components with respect to each other. Thereby an overall phase retardation is realized. The grating material must show a zero extinction coefficient in the required wavelength range to avoid absorption effects.
In section 1, the design and fabrication of a nano-optical wave plates with application in the visible wavelength range is discussed. In section 2, the optical properties of a fabricated

sample are investigated. The main structure deviations and their influence on the optical properties are presented in section 3. A first approach for an in-situ process control is shown in section 4. Finally, the results are summarized in section 5.

1. DESIGN AND FABRICATION

1.1 Effective Media Approximation (EMA)

Sub-wavelength gratings have to fulfill several requirements regarding their specific grating parameters. By using a grating structure, diffraction is possible. Typically diffraction is unwanted and solely the transmission of the zeroth order is desired. To suppress higher diffraction orders ($m > 0$) in the limiting case the diffraction angle θ_m has to be equal 90° for the first diffraction order ($m = 1$), which correspond to evanescent waves. Thus the grating period p in dependence of the incident wavelength λ has to fulfill the relation:

$$n_S \sin\theta_m + n_A \sin\alpha = m\frac{\lambda}{p},$$
$$\theta_{\pm 1} = 90° \rightarrow p_{ZOG} < \frac{\lambda}{2n_S}. \quad (1)$$

This so called zero-order-grating period p_{ZOG} further depends on the refractive index of the substrate n_S and ambient medium n_A as well as the incident angle α of the incoming light. In figure 1 this situation is illustrated. For incident light at $\alpha = 0°$ in the visible wavelength range ($\lambda \geq 400nm$) and a fused silica substrate ($n_S \approx 1.47$) the grating period should be smaller than 270nm. Here a grating period of 100nm is chosen and thus, no diffraction orders appear for arbitrary angles of incidence.

To describe the resulting phase shift the grating can be supposed as an effective, birefringent medium [6] for sufficiently smaller grating periods than the incident wavelength. In general the chosen grating period should be smaller than p_{ZOG} to operate in the sub-wavelength regime. The refractive indices n_{TE} and n_{TM} depend on the orientation of the polarization plane of the incident light [7]:

$$n_{TE} = \left(f\, n_R^2 + (1-f)\, n_A^2\right)^{1/2}, \quad (2)$$

$$n_{TM} = \left(\frac{f}{n_R^2} + \frac{1-f}{n_A^2}\right)^{-1/2}, \quad (3)$$

$$\text{with } f = \frac{d}{p}. \quad (4)$$

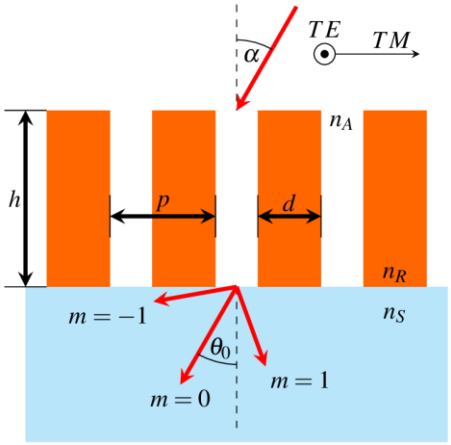

1:Sub-wavelength grating and corresponding grating parameters.

The refractive index of the grating ridges is n_R and the ratio between ridge width d and grating period p defines the duty cycle f. For a birefringent layer with the height h the induced phase shift Δϕ for polarized light can be calculated as followed:

$$\Delta\phi = \frac{2\pi h}{\lambda}(n_{TE} - n_{TM}) \quad (5)$$

The phase shift shows the typical indirect proportionality – for smaller wavelength the phase shift is higher. The EMA provide a first impression of the main design parameters: ridge material, duty cycle and grating height. For efficient gratings a large refractive index difference between ridge and surrounding media is beneficial. For this reason the ridges of our fabricated gratings consists of titanium dioxide (TiO_2) combined with air as ambient medium.

Furthermore a duty cycle of f=0.62 results in a maximum phase shift for a given grating height. Finally the grating height is the most important parameter, a higher grating structure results in a higher total phase shift.
For a first design a quarter-wave plate for λ=532nm is targeted, aiming at various available laser applications. Therefore, a grating height of 216nm in combination with f=0.62 duty cycle and TiO2 as ridge material is required. In figure 2 the corresponding phase shift as function of the wavelength is illustrated.

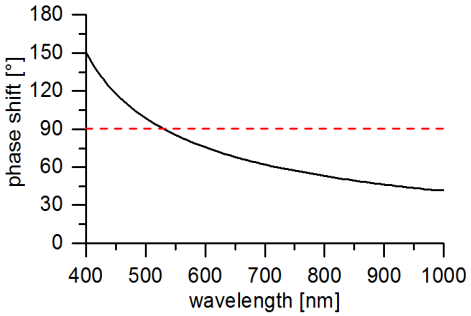

2: Phase shift (EMA) for a TiO_2 grating with 0.62 duty cycle and 216nm grating height.

1.2 Modified self-aligned double patterning process (SADP)

The nano-optical wave plates were fabricated by a modified self-aligned double patterning process (SADP) in combination with character projection electron beam lithography as shown in figure 3. Initially a layer stack consisting of polymer, chromium hard mask and electron beam resist is manufactured by spin coating and ion beam deposition (IBD) on a fused silica substrate (figure 3a). The height of the polymer layer defines the maximum achievable grating height. The Vistec SB350-OS electron beam writer generates the required grating structure in the resist (figure 3b) via character projection. To achieve the required ridge width the resist is trimmed via low energy reactive ion beam etching (RIBE) with oxygen at an angle of 45° to the substrate. Following this, the structure is etched into the chromium and polymer using ion beam etching (IBE) and RIBE (figure 3c). The template is coated with TiO_2 through atomic layer deposition (ALD) [8], see figure 3d. Subsequently due to the high aspect ratio it is difficult to remove the upper and lower horizontal TiO_2 layers on the template and substrate, respectively. Through a planarization process [9] it is possible to remove the upper horizontal layer and the remaining polymer. Therefore the whole structure is covered with polymer (figure 3e) and afterwards etched via IBE under an angle of 20° into the substrate. Here, the etch rates for the polymer and TiO_2 are nearly the same (see figure 4) and a flat top surface of the TiO_2-structure can be obtained (figure 3f). Finally, the remaining polymer is removed via RIBE. The result is a u-shaped grating structure with a period of 200nm (figure 3g). It is expected that this deviation from an ideal grating affects the optical performance.

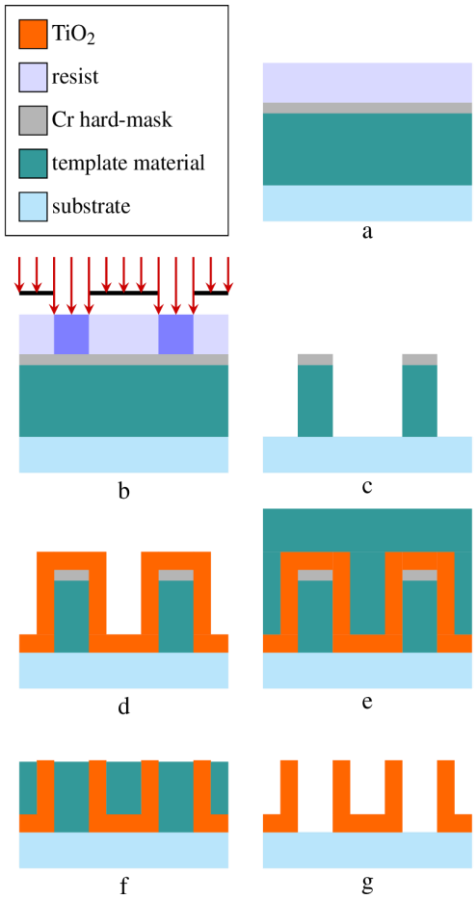

3: SADP and planarization process.

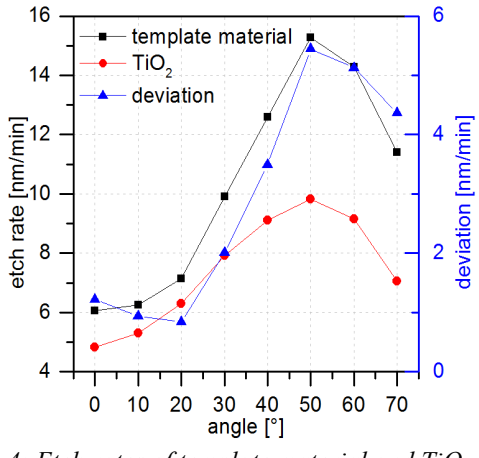

4: Etch rates of template material and TiO_2 for varying angles.

1.3 Design for the u-shaped grating structure

The u-shaped structure possesses an expanded bottom part, which differs from the ideal duty cycle and period. In order to understand the influence of a u-shaped grating structure a rigorous analysis of the pattern using a rigorous coupled wave analysis (RCWA) has been performed [10]–[12]. Compared to EMA the RCWA offers additional advantages such as a wavelength dependent solution and the possibility to consider structure deviations, which can occur during the fabrication. Furthermore the ratio of the field amplitude for TE and TM polarized light is important. For a phase plate, polarization independent amplitude transmission properties are required. The result of a RCWA simulation for varying duty cycles and grating heights for the phase shift and amplitude ratio is presented in figure 5a and 5b. The contour lines highlight the tolerance regions of $\pm 5\%$. This analysis leads to an optimal grating height of $(260 \pm 5)\text{nm}$ and a duty cycle of $0.66 + 0.09/-0.01$. In figure 5c solely the phase shift for the amplitude ratio within the tolerance region is shown. The green dot marks the chosen parameter set.

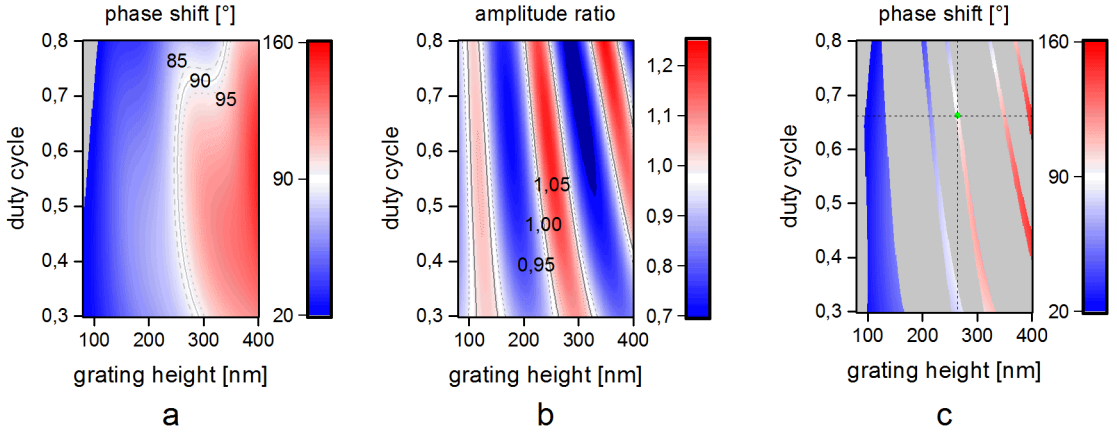

5: RCWA results for a u-shaped grating. The contour lines highlight the tolerance regions for the phase shift (a) and amplitude ratio (b). In figure (c) the phase shift is shown for the amplitude ration within their tolerance region and the green dot marks the chosen parameter set of 260nm grating height and 66nm ridge width.

The small tolerance for the grating height (±5nm) and the aspect ratio (ratio of height and ridge width) of about five in combination with the small period is challenging for the fabrication process [5]. The wavelength dependency of phase shift and amplitude ratio for a parameter set of 260nm grating height and 66nm ridge width is displayed in figure 6. The fluctuation of the amplitude ratio over the wavelength is a result of wavelength dependent reflection of the TE polarized light. The resonant peak near λ=450nm is induced by the lower horizontal TiO_2 ridge, which acts as resonant waveguide for the TM polarized light. For applications at this wavelength a reduced grating period of 160nm shifts this resonance below 400nm wavelength.

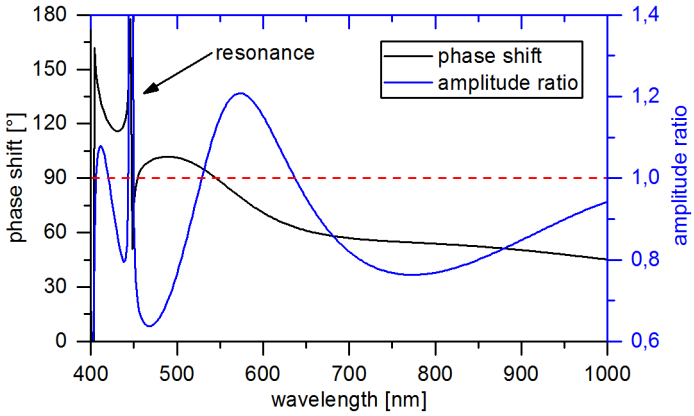

6: Phase shift and amplitude ratio for a u-shaped grating (260nm grating height and 0.66 duty cycle).

2. MEASUREMENT

The wavelength dependent phase difference of a fabricated nano-optical quarter-wave plate was measured by a Sentech SE850 ellipsometer in transmittance. For λ=532nm a phase shift of 45° and an amplitude ratio of 0.77 was measured, which is lower than the RCWA prediction. In comparison with figure 6 the trend of the amplitude ratio of the measured sample is shifted towards lower wavelengths. The grating resonance occurs at λ=416nm, not matching with the RCWA results.

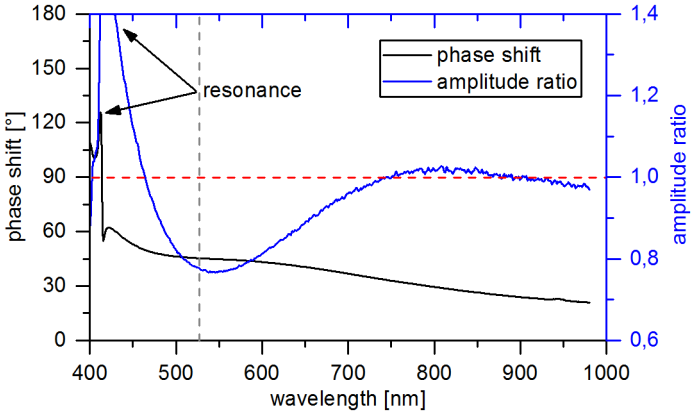

7: Measured phase shift and amplitude ratio with the Sentech SE850 ellipsometer.

To obtain information of the grating structure, cross section images by scanning electron microscope (SEM) were recorded (see figure 8a). The sample shown in figure 8b was prepared by a focused ion beam (FIB). The cross section images reveal several structure deviations like ridge tilt, ridge displacement, chamfers and a reduced grating height. The influence of these deviations are investigated in the following section.

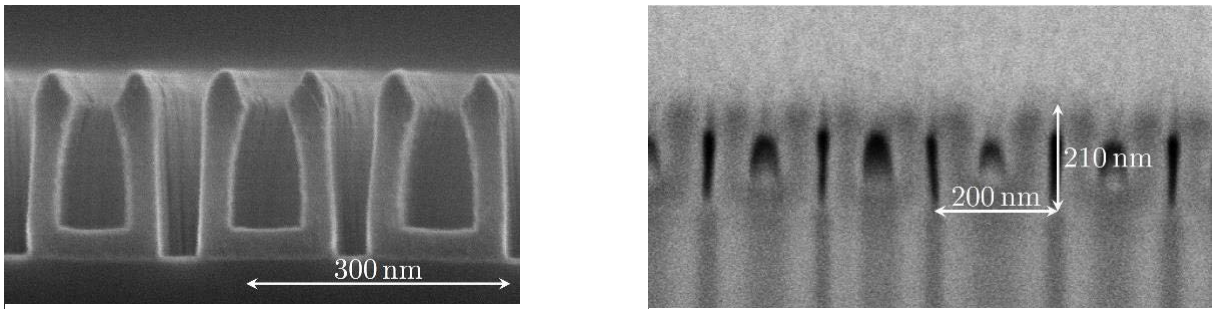

a b

8: Cross section image showing structure deviations. The sample in figure (b) was prepared via FIB and is coated with platinum as conducting layer.

3. STRUCTURE DEVIATIONS

During fabrication, several main structure deviations occurred like ridge tilt, ridge displacement, chamfers and overall lower grating height (see figure 9). The estimated deviations of the measured sample in figure 8b are 3° ridge tilt, 15nm ridge displacement, 50° chamfer angle and a grating height of 210nm. The latter is caused by over-etching during planarization. The measurement of the covering polymer layer thickness is difficult due to its complex fluidic behavior during spin coating. In combination with the approximate etch rates, it is not trivial to find the ideal process time to remove all of the upper horizontal TiO_2 layer. A lower grating height lowers

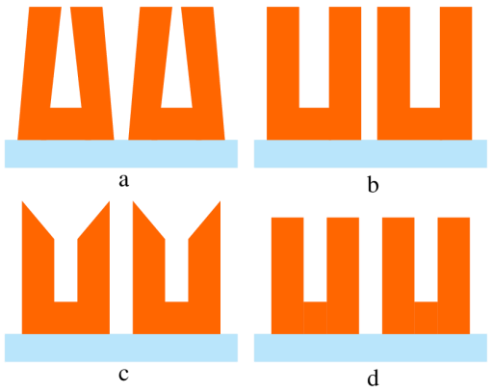

9: Structure deviations: (a) ridge tilt, (b) ridge displacement, (c) chamfers and (d) lower grating height.

the overall phase shift. Next, a grating ridge tilt arises by an undercut of the template structure. During the RIBE etch of the template the undercut develops due to a slight divergence of the ion beam. For the SADP process the ridge displacement is a consequence of a differing structure width in the template. The resulting tilt and displacement is equivalent to a variation of the duty cycle over the grating height and leads to a non-ideal duty cycle, which varies the phase shift. At last the angle dependent etch rate of the planarization process (see figure 4) leads to chamfers on top of the ridges and lower the phase shift. The observed deviations are included in a renewed RCWA calculation. The resulting phase shift and amplitude ratio is displayed in figure 10. The grating resonance occurs at λ=416nm, now matching with the measurement. At λ=532nm a phase shift of 54° and an amplitude ratio of 0.89 is calculated. In comparison to figure 6 the amplitude ratio is shifted towards lower wavelengths but it does not match perfectly with the measurement data in figure 7. Additionally the determined phase shift and amplitude ratio for λ=532nm is higher than the measured values. This indicates further structure or material deviations, which are not considered in the RCWA solution. For example local refractive index inhomogeneity or line edge roughness [13] can influence the optical performance of this nano-optical elements.

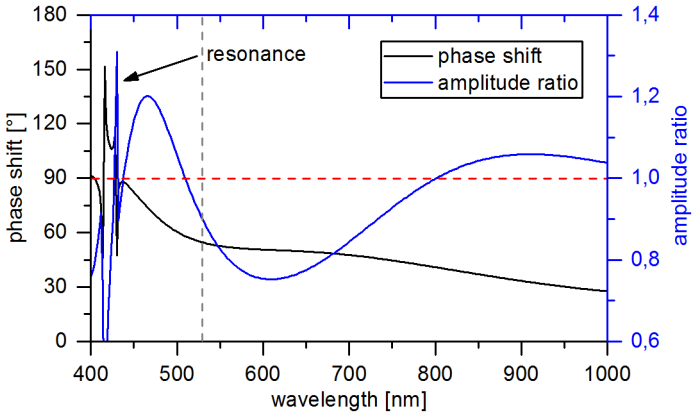

10: Phase shift and amplitude ratio of a u-shaped grating including the observed structure deviations, determined via RCWA.

4. IN-SITU PROCESS CONTROL

To improve the optical performance an in-situ process control of the optical properties would be a huge advantage. Therefore, the evolution of the phase shift for the different fabrication processes, starting with the planarization, were determined via RCWA (see figure 11).
At first the polymer layer, covering the whole structure, is etched via IBE. Due to the isotropic properties of the polymer, no additional phase shift is induced. The small phase shift fluctuations (till marker 1) are be caused by a Fabry-Pérot resonance within the layer. At marker 1 the polymer on top of the structure is removed. By proceeding the IBE etching the TiO_2 layer, forming a birefringent structure, is reduced and as a result the phase drops significant till the entire material is removed (marker 3). At marker 2 the horizontal TiO_2 layer is removed and this is the ideal point to stop the IBE etching. The plateau for the phase shift at marker 2 can be used as stopping criteria. Next, the polymer between the TiO_2 ridges is removed via RIBE etching, resulting in a rising of the phase shift till marker 4. At this point all polymer is removed and the process should be stopped. However if continued, the grating height is further reduced, resulting in a reduction of the phase shift until all material is removed (marker 5). The change of the slope can be used as a stop criteria for the RIBE process. To verify the RCWA calculation the fabrication processes of a sample were stopped several times to measure the phase shift. The results are displayed in figure 11 as read dots. The trend correlates to the simulation, the general difference can be explained by the discussed structure deviations. By intentionally increasing the starting template height, and

thereby the final ridge height, the phase shift can be fine-tuned by an additional etching step. Furthermore the phase shift reduction due to the structure deviations can be compensated.

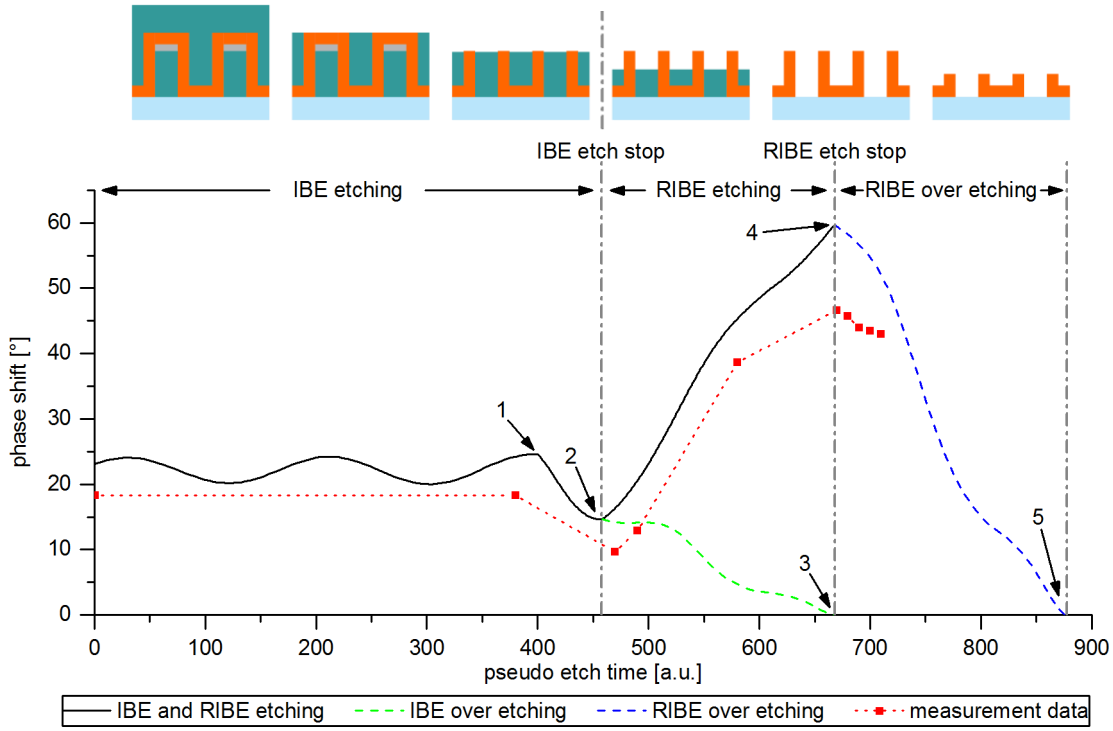

11: Evolution of the phase shift for the planarization process, determined via RCWA.

For the future we want to integrate an in-situ phase measurement setup into the Oxford Ionfab 300Plus etch and deposition facility to use the described in-situ process control for the fabrication of nano-optical wave plates.

5. CONCLUSION

In this contribution we presented the design and fabrication of nano-optical wave plates for the visible and near infrared wavelength regime. The observed structure deviations ridge tilt, ridge displacement, chamfers and lower grating height lead to a reduced phase shift, and the amplitude ratio and grating resonance is shifted towards lower wavelengths. At λ=532nm a phase shift of 45° and an amplitude ratio of 0.77 was obtained. A renewed RCWA calculation including the main deviations lead to a better understanding of the obtained optical properties. The presented in-situ process control enables a fine-tuning of the phase shift and in addition the influence of structure deviations can be compensated.

REFERENCES

[1] P. C. Deguzman and G. P. Nordin, “Stacked subwavelength gratings as circular polarization filters.,” *Appl. Opt.*, vol. 40, no. 31, pp. 5731–7, Nov. 2001.

[2] T. Glaser, S. Schröter, H. Bartelt, H.-J. Fuchs, and E.-B. Kley, “Diffractive optical isolator made of high-efficiency dielectric gratings only,” *Appl. Opt.*, vol. 41, no. 18, p. 3558, Jun. 2002.

[3] T. Weber, T. Kasebier, S. Kroker, E.-B. Kley, and A. Tünnermann, “High frequency binary amorphous silicon grating working as wire grid polarizer for UV applications,” *Proc. SPIE - Int. Soc. Opt. Eng.*, vol. 8270, p. 82700F–82700F–6, Feb. 2012.

[4] T. Weber, T. Käsebier, E.-B. Kley, and A. Tünnermann, “Broadband iridium wire grid polarizer for UV applications.,” *Opt. Lett.*, vol. 36, no. 4, pp. 445–447, Feb. 2011.
[5] T. Siefke, S. Kroker, K. Pfeiffer, O. Puffky, K. Dietrich, D. Franta, I. Ohlídal, A. Szeghalmi, E.-B. Kley, and A. Tünnermann, “Materials Pushing the Application Limits of Wire Grid Polarizers further into the Deep Ultraviolet Spectral Range,” *Adv. Opt. Mater.*, vol. 4, no. 11, pp. 1780–1786, Nov. 2016.
[6] S. M. Rytov, “Electromagnetic Properties of a Finely Stratified Medium,” *Sov. Phys. JETP*, vol. 2, no. 3, pp. 466–475, 1956.
[7] J. H. Schmid, P. Cheben, P. J. Bock, R. Halir, J. Lapointe, S. Janz, A. Delage, A. Densmore, J.-M. Fedeli, T. J. Hall, B. Lamontagne, R. Ma, I. Molina-Fernandez, and D.-X. Xu, “Refractive Index Engineering With Subwavelength Gratings in Silicon Microphotonic Waveguides,” *IEEE Photonics J.*, vol. 3, no. 3, pp. 597–607, Jun. 2011.
[8] M. Ritala, M. Leskela, L. Niinisto, and P. Haussalo, “Titanium isopropoxide as a precursor in atomic layer epitaxy of titanium dioxide thin films,” *Chem. Mater.*, vol. 5, no. 8, pp. 1174–1181, Aug. 1993.
[9] T. Siefke, “Optimization of double patterning for DUV tungsten wire grid polarizer,” Friedrich-Schiller-Universität Jena, 2013.
[10] M.G.Moharam and T.K.Gaylord, “Rigorous coupled-wave analysis of planar-grating diffraction,” *J. Opt. Soc. Am.*, vol. 71, no. 7, p. 811, Jul. 1981.
[11] P. Lalanne and J.-P. Hugonin, “High-order effective-medium theory of subwavelength gratings in classical mounting: application to volume holograms,” *J. Opt. Soc. Am. A*, vol. 15, no. 7, p. 1843, Jul. 1998.
[12] J. Hench and Z. Strakoš, “The RCWA method-a case study with open questions and perspectives of algebraic computations,” *Electron. Trans. Numer. Anal.*, vol. 31, pp. 331–357, 2008.
[13] T. Siefke, C. B. Rojas Hurtado, J. Dickmann, M. Heusinger, and S. Kroker, “Simulation of the Influence of Line Edge Roughness on the Performance of Deep Ultra Violet Wire Grid Polarizers,” *SPIE Optical metrology*, Munich, 26.06.-28.06.2017.

CONTACTS

Carsten Stock carsten.stock@uni-jena.de
Thomas Siefke thomas.siefke@uni-jena.de
Uwe Zeitner uwe.zeitner@iof.fraunhofer.de
Ernst-Bernhard Kley ernst-bernhard.kley@uni-jena.de